Infiltration into unsaturated reinforced slopes with nonwoven geotextile drains sandwiched in sand layers

J. N. Thuo[1], K. H. Yang[2] and C. C. Huang[3]

[1]*Graduate Student, Department of Civil and Construction Engineering, National Taiwan University of Science and Technology, Taipei, Taiwan, Telephone: +886 928441052; Telefax: +886 227376606; E-mail: D10305813@mail.ntust.edu.tw*
[2]*Associate Professor, Department of Civil and Construction Engineering, National Taiwan University of Science and Technology, Taipei, Taiwan, Telephone: +886 227301227; Telefax: +886 227376606; E-mail: khy@mail.ntust.edu.tw (Corresponding author)*
[3]*Professor, Department of Civil Engineering, National Cheng Kung University, Tainan, Taiwan, Telephone: +886 62757575-63160; Telefax: +886 62358542; E-mail: samhcc@mail.ncku.edu.tw*

Received 19 November 2014, revised 11 April 2015, accepted 03 June 2015, published 16 September 2015

ABSTRACT: The use of nonwoven geotextile drains in geosynthetic-reinforced soil (GRS) structures has been suggested to facilitate the dissipation of pore water pressure. It has also been recognised that the nonwoven geotextile may retard water penetration due to the capillary barrier effect under unsaturated soil conditions and can function as a drainage material only once the soil immediately above it is nearly saturated. In this study, numerical models of unsaturated slopes with nonwoven geotextile drains, subjected to rainfall infiltration were developed to investigate the unsaturated hydraulic behaviour and stability of slopes constructed with nonwoven geotextile drains in thin layers of highly permeable sand (i.e. sand cushions). The numerical models were first validated for their suitability for modelling water flow and the capillary barrier effect within unsaturated soils using the experimental results from a one-dimensional soil column infiltration test and full-scale infiltration tests. Next, a series of numerical simulations of unsaturated slopes with and without sand cushions and under different infiltration conditions were performed. The numerical results indicated that the sand cushions reduced the development of the capillary barrier effect by acting as an intermediate material between the backfill and the nonwoven geotextile, which bridged the gap between two materials with very different unsaturated hydraulic characteristics. The reduction of the development of the capillary barrier effect led to the accumulation of pore water pressure above the nonwoven geotextile being effectively dissipated downward. The sand cushions also acted as additional drain layers to facilitate the drainage of water within the slope system. Thus, the inclusion of sand cushions enhanced the local slope stability for soils above the top geotextile layer. Based on the numerical results, methods for determining the occurrence of the capillary barrier effect are identified from the literature and discussed.

KEYWORDS: Geosynthetics, Unsaturated flow, Capillary barrier effect, Infiltration, Nonwoven geotextile, Sand cushion

REFERENCE: Thuo, J. N., Yang, K. H. and Huang, C. C. (2015). Infiltration into unsaturated reinforced slopes with nonwoven geotextile drains sandwiched in sand layers. *Geosynthetics International*, **22**, No. 6, 457–474. [http://dx.doi.org/10.1680/jgein.15.00026]

1. INTRODUCTION

The backfill material forms one of the major constituents of geosynthetic-reinforced soil walls and slopes and accounts for 30–40% of their cost (Christopher and Stuglis 2005; Raisinghani and Viswanadham 2011). Design guidelines (Elias *et al*. 2001; AASHTO 2002; Berg *et al*. 2009; NCMA 2010) limit the use of fine-grained soils as backfill material within the reinforced zone. Figure 1 shows the gradation limits specified in the design guidelines. In addition to the gradation limits, the plasticity index of the backfill is also specified (PI$\leq$6 and 20 for walls and slopes, respectively). However, to reduce the construction cost of geosynthetic-reinforced soil (GRS) structures and minimise the transportation cost and environmental impact associated with the disposal of the excavated soil, locally available soils with relatively low hydraulic conductivity (usually referred to as marginal fills) have been used as alternative backfills.

It has been reported that the low draining capacity of fine soils compromised the performance of reinforced soil walls upon rainfall infiltration because of the build-up of

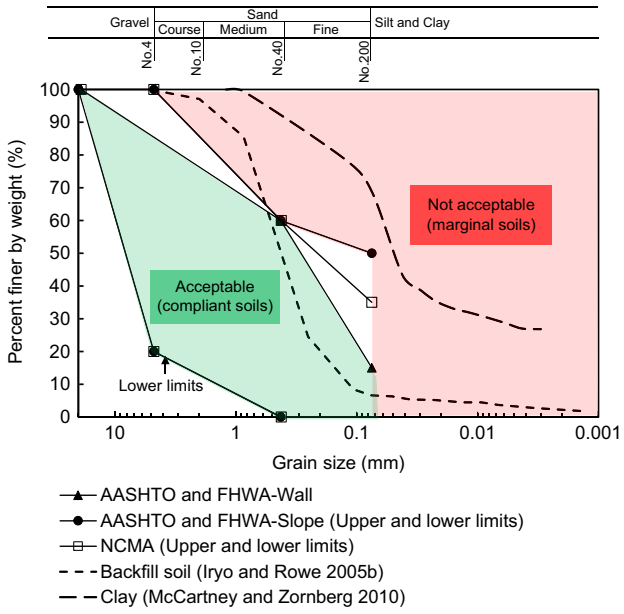

Figure 1. Grain size distribution of backfill in GRS structures as recommended by design guidelines and the soils used in this study

pore water pressure (Zornberg and Mitchell 1994; Mitchell and Zornberg 1995; Yoo and Jung 2006; Koerner and Koerner 2013; Valentine 2013; Santos *et al*. 2014). The use of geosynthetic drains (nonwoven geotextile or geocomposites) for improving the drainage capacity of marginal fills has been suggested (Mitchell and Zornberg 1995; Christopher *et al*. 1998). Several studies have been conducted to better understand the drainage performance of soil–geosynthetic systems. Geosynthetic drains play a significant role in enhancing pore water pressure dissipation and increasing the stability of low-permeability backfill slopes under saturated soil conditions (Mitchell and Zornberg 1995; McKean and Inouye 2001; Raisinghani and Viswanadham 2010).

Many studies have shown that nonwoven geotextiles act as a drainage material in situations where pore pressures are positive. However, considering that during the construction of earth-retaining structures in the field, backfill soils are compacted at ±2% of the optimum moisture content, these soils are usually unsaturated and negative pore pressure (i.e. suction) is generated (Yoo and Jung 2006; Huang *et al*. 2008; Liu *et al*. 2012; Huang and Lo 2013; Valentine 2013). In unsaturated soil–nonwoven geotextile systems, nonwoven geotextiles have been reported to function as a moisture barrier rather than a drainage material owing to the capillary barrier effect, and this may obstruct seepage flow under some circumstances (Iryo and Rowe 2003, 2004, 2005a, 2005b; Bathurst *et al*. 2007, 2009; Siemens and Bathurst 2010; Zornberg *et al*. 2010; Bouazza *et al*. 2013).

Zornberg *et al*. (2010) stated that the development of geosynthetic capillary barriers may benefit a number of geotechnical and environmental applications (e.g. prevention of frost heave and moisture migration in pavement, application of alternative cover system in landfill design, and increase of moisture storage in agriculture and turf systems) or have adverse impact on geotechnical application (e.g. moisture accumulation in slopes and reinforced earth structures). The pore pressure increase could weaken the soil in the vicinity of the geotextile and at the interface between the soil and the geotextile, leading to soil deformation or even soil failure. Failures caused by the capillary barrier effect have been reported by many studies (Richardson 1997; Garcia *et al*. 2007; Mancarella *et al*. 2012). Thus, Bouazza *et al*. (2013) and Iryo and Rowe (2004) suggested that considerable care is required when selecting nonwoven geotextiles for use within soil structures, to avoid the undesirable development of increased water content. Methods including placing geotextile in the form of strips (Garcia *et al*. 2007) and using wicking geotextile (Azevedo and Zornberg 2013) have been introduced to minimise the capillary barrier effect and facilitate water drainage.

The concept of sandwiching nonwoven geotextile drains in thin layers of sand (known as sand cushion or sandwich technique) has been applied to accelerate pore water pressure dissipation, increase soil–geotextile system's drainage capacity under saturated conditions (Raisinghani and Viswanadham 2010), reduce the surficial intrusion and long-term clogging in the nonwoven geotextiles by fine-grained soils (Lin and Yang 2014), enhance pullout resistance (Abdi and Zandieh 2014), and improve the strength and deformation characteristics of reinforced clay by improving the soil–reinforcement interface shear strength (Unnikrishnan *et al*. 2002; Abdi *et al*. 2009). In particular, sand cushions have been used in drainage installation in Taiwan to reduce the possibility of long-term clogging of nonwoven geotextile drains (Figure 2). Although intensive studies have been performed on water infiltration into soil–geotextile systems, the unsaturated hydraulic performance of soil–sand cushion–geotextile drain systems during rainfall infiltration has not been comprehensively studied. For the effective and appropriate use of sand cushions, studies of the characteristics of these systems are necessary.

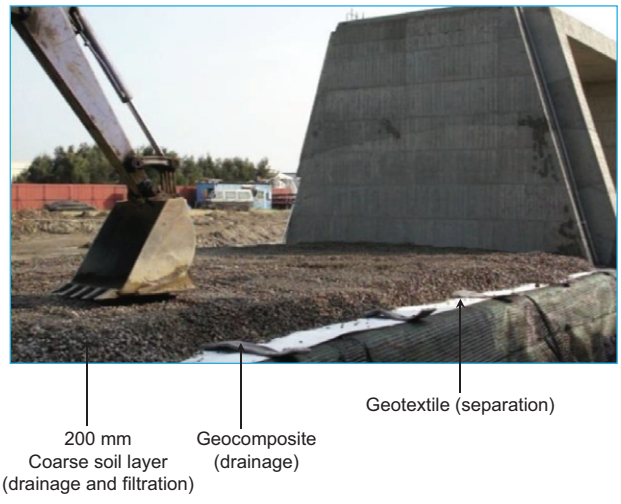

Figure 2. GRS wall construction: provision of a 200 mm thick layer of coarse soil cushion above drainage layers prior to placing of locally available backfill soil (courtesy of Gold-Joint Industry Company)

The main objectives of this study were twofold: to examine the suitability of finite-element formulations for modelling the capillary barrier effect and to investigate unsaturated soil hydraulic behaviour when geotextile is sandwiched between sand layers, especially to evaluate the effect of sand cushions on the development of the capillary barrier effect. First, a one-dimensional model was developed and calibrated using experimental results for a one-dimensional homogeneous clay-nonwoven geotextile system subjected to water infiltration. Second, numerical experiments on unsaturated slopes with nonwoven geotextile drains with and without sand cushions were conducted to provide insights into the hydraulic behaviour of such systems. Based on the findings of the numerical studies, the hydraulic behaviour of unsaturated soil–nonwoven geotextile systems subjected to infiltration and the effect of sand cushions are discussed. The results obtained from this study are expected to provide insightful information on the unsaturated flow within GRS structures.

2. REVIEW OF GEOSYNTHETIC CAPILLARY BARRIERS

To determine the factors influencing the occurrence of the capillary barrier effect, a review of methods used to determine whether the capillary barrier effect will occur was conducted and presented in this section. The methods discussed in this section will be examined based on the infiltration simulation results presented in Section 5.4. Readers are also referred to Zornberg *et al.* (2010) for a comprehensive review of the current state of knowledge on geosynthetic capillary barriers.

The capillary barrier effect occurs when a fine-grained soil layer overlies a coarse material (coarse-grained soil or nonwoven geotextile). The hydraulic characteristics of fine and coarse materials are generally contrastive (the coarse material has smaller water entry values and a steeper hydraulic conductivity function) (Iryo and Rowe 2005a; Zornberg *et al.* 2010). The main effect of the capillary barrier effect is that a measurable amount of water will not flow from the fine-grained soil to the underlying nonwoven geotextile drain until a critical suction threshold is reached. In this condition, nonwoven geotextile acts as a water barrier and leads to an increase in the pore water pressure in the soils immediately above it, in contrast to its behaviour under saturated conditions (McCartney and Zornberg 2010; Bouazza *et al.* 2013). Such increase in the pore pressure could also occur when the geotextile is used for filtration, separation, or reinforcement.

Research has suggested that the water entry suction value obtained from the water retention curve (WRC) of the underlying coarse material can be used to determine the critical (or threshold) matric suction value at which water starts flowing into the underlying coarse material (Stormont and Morris 2000; Iryo and Rowe 2005a; McCartney and Zornberg 2010). At suctions greater than the water entry suction, the available water pathways are discontinuous and impeding water flow into the underlying material; as a result, the capillary barrier effect occurs. By contrast, at suctions lower than the water entry suction, the water pathways are connected; consequently, water flows into the underlying material and the capillary barrier effect does not occur. Fredlund (2006) stated that the water entry suction corresponds to the residual matric suction ψ_r; hereafter, in this paper, the suction corresponding to the water entry value in the WRC is referred to as ψ_r.

Zornberg *et al.* (2010) indicated even if water infiltrates the overlying fine-grained material during precipitation events and reaches the interface of the two materials, it can enter the underlying coarse-grained material only at a very slow rate. Therefore, water accumulates at the interface until the suction at the interface reaches a value at which the hydraulic conductivity of the coarse-grained material is no longer below that of the fine-grained material. In other words, a measurable amount of water will not infiltrate the underlying coarse layers until the suction decreases to the ψ_b value at which the conductivity of both layers is identical at the interface (Iryo and Rowe 2005b; McCartney and Zornberg 2010; Bouazza *et al.* 2013). Hereafter, the suction at which the hydraulic conductivity functions of the two materials intersect is denoted by ψ_b, and the corresponding hydraulic conductivity is represented by k_b. In summary, the capillary barrier effect occurs under the following condition

$$\psi_{initial} > \min(\psi_r, \psi_b) \tag{1}$$

where $\psi_{initial}$ is the initial suction, ψ_r and ψ_b are defined previously.

The hydraulic performance of unsaturated soil–geotextile systems after capillary breakthrough – passage of the wetting front through the geotextile layer – was discussed by Iryo and Rowe (2004). They found that the development of pore pressure profile was related to the relationship among the infiltration rate q, saturated hydraulic conductivity of the soil $k_{sat\ soil}$, and nonwoven geotextile $k_{sat\ geotextile}$. In the ponding water case, when $k_{sat\ geotextile} < k_{sat\ soil}$, both the soil and geotextile are close to the saturated state after capillary breakthrough, and the built-up pore pressure above the geotextile is maintained since the hydraulic conductivity of the geotextile is smaller than that of the soil. However, if $k_{sat\ geotextile} > k_{sat\ soil}$, the geotextile is more permeable than the soil under saturated conditions, and the built-up pore pressure may dissipate after capillary breakthrough. In the no-ponding case (under infiltration case) where $k_{sat\ geotextile} > k_{sat\ soil}$ and infiltration rate $q < k_{sat\ soil}$, when the wetting front passes through the geotextile, pore pressures in the soil *below* the geotextile layer increase but do not become positive because the inflow flux is smaller than the outflow flux ($q < k_{sat\ soil}$). Thus, $k_{geotextile}$ will decrease with depth from its saturated value at the geotextile's upper surface to some lower value at geotextile's lower surface. The built-up pore pressure above the geotextile layer dissipates but a relative small pore pressure discontinuity remains at the soil-geotextile interface.

3. NUMERICAL VERIFICATION OF CAPILLARY BARRIER EFFECT

3.1. The experiment

McCartney and Zornberg (2010) performed a series of one-dimensional soil column tests to investigate the effect of infiltration and evaporation on geosynthetic capillary barrier performance. The test soil column was a 203-mm-diameter cylindrical polyvinyl chloride (PVC) tube filled with unsaturated clay underlain by a geocomposite drainage layer (GDL).

The soil used in the tests was classified as low-plasticity clay (CL) according to the Unified Soil Classification System (ASTM D2487) with basic properties shown in Table 1. The soil specimen (column A) in one of column tests was 1350 mm high, and it was compacted in 25 mm lifts using a pneumatic piston compactor at an optimal gravimetric water content of $\omega = 11.5\%$ according to the standard proctor compaction test (ASTM D698). The soil column was subjected to a series of uniform infiltration of water from the top at a rate $q = 3.4 \times 10^{-9}$ (m/s) ($= 0.00005\ k_{\text{sat soil}}$). Figure 3 shows the hydraulic characteristics of the clay and geotextile (a component of the GDL), determined experimentally by McCartney and Zornberg (2010). The moisture content profiles in the soil column were monitored using time domain reflectometry (TDR), as shown in Figure 4. No matric suction information was reported for this test.

3.2. Numerical simulation

Transient seepage analysis was conducted to examine the unsaturated hydraulic behaviour of the fine-grained soil–nonwoven geotextile system subjected to infiltration, with specific interest in the suitability of finite-element formulations for modelling the capillary barrier effect. SEEP/W software (Geo-Slope 2009) based on finite-element code was used to solve Equation 2 which represents the two-dimensional form of the governing equation for transient flow within an unsaturated medium; as the two-dimensional form was derived by Richards (1931) from Darcy's law and the continuity equation.

$$k_x \frac{\partial^2 h}{\partial x^2} + k_y \frac{\partial^2 h}{\partial y^2} = \frac{\partial \theta}{\partial t} = m_w \rho_w \boldsymbol{g} \frac{\partial h}{\partial t} \qquad (2)$$

where k_x and k_y represent the hydraulic conductivities in the x- and y-direction, h is the total hydraulic head available for flow, θ is the volumetric water content, m_w is the coefficient of water volume change (slope of the water characteristic curve), ρ_w is the density of water, $\boldsymbol{g}$ is the acceleration of gravity, and t is the time.

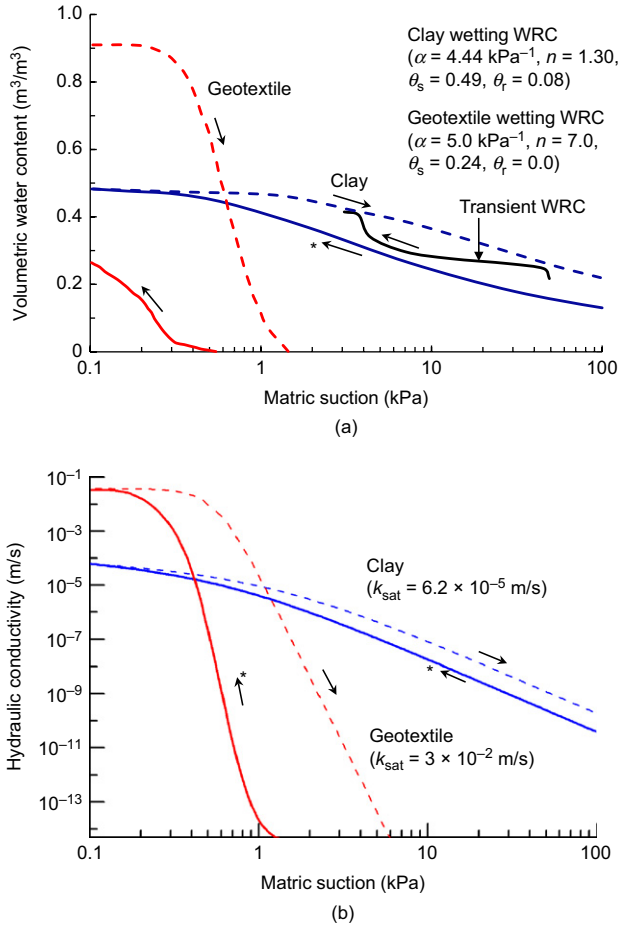

Figure 3. Hydraulic characteristics for clay and nonwoven geotextile: (a) water retention curves; (b) *k*-functions. Note: arrows denote the drying and wetting processes. Star marks indicate the wetting water retention curves and *k*-functions estimated in this study and the curves without star marks were adopted from McCartney and Zornberg (2010)

Table 1. Soil hydraulic and shear strength properties used in the simulation

Parameter	Clay[a]	Backfill[b]	Sand cushion[c]
Saturated hydraulic conductivity, k_{sat} (m/s)	6.2×10^{-5}	1.3×10^{-5}	1.0×10^{-2}
Saturated volumetric water content, θ_s	0.49	0.47	0.38
Residual volumetric water content, θ_r	0.08	0.04	0.05
van Genuchten fitting parameter, α^w (kPa^{-1})	4.44	0.6	0.72
van Genuchten fitting parameter, n	1.30	1.80	3.16
Friction angle, ϕ' (°)	–	40	40
Friction angle relative to matric suction, ϕ^b (°)	–	16	16
Cohesion, c' (kPa)	–	0	0

[a]Deduced from McCartney and Zornberg (2010).
[b]Deduced from Iryo and Rowe (2005b).
[c]Deduced from Iryo and Rowe (2005a) but increased the k_{sat} value from 10^{-4} to 10^{-2} m/s.

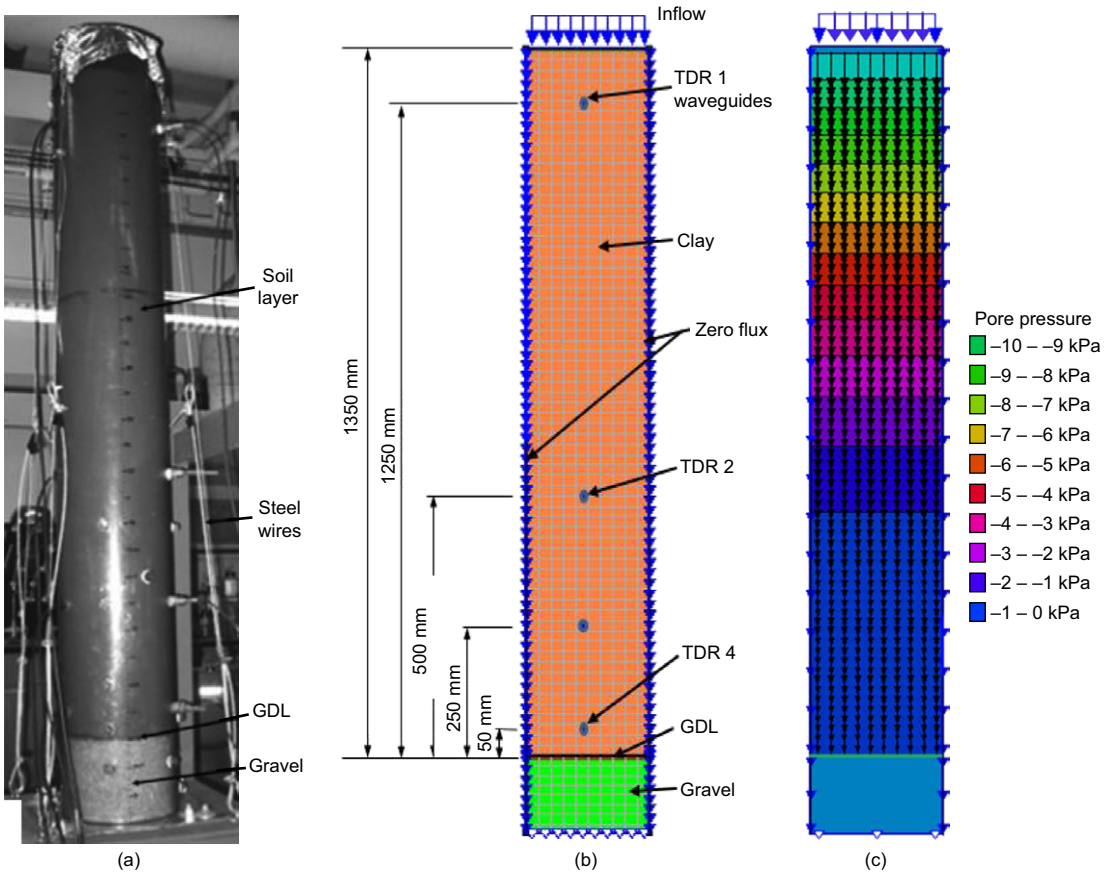

Figure 4. Experiment setup and numerical model of the soil column infiltration test: (a) photo (McCartney and Zornberg 2010; © 2008 Canadian Science Publishing or its licensors. Reproduced with permission); (b) numerical model; (c) seepage velocity vectors and pore pressure contour

The van Genuchten (1980) model was used to fit the WRCs and to predict the hydraulic conductivity functions.

$$\Theta = \frac{\theta - \theta_r}{\theta_s - \theta_r} = \left(\frac{1}{1 + (\alpha\psi)^n}\right)^m \quad (3)$$

$$k = k_{sat}\Theta^{1/2}[1 - (1 - \Theta^{1/m})^m]^2 \quad (4)$$

where Θ is the normalised volumetric water content, θ_s is the saturated volumetric water content, θ_r is the residual volumetric water content, ψ is the suction (positive value), k is the hydraulic conductivity, k_{sat} is the saturated hydraulic conductivity, and α, n, and m are curve-fitting parameters, with $m = 1 - 1/n$ being typically assumed.

The curve-fitting parameters of the drying WRC of the clay ($\alpha^d = 2.22\ kPa^{-1}$, $n^d = 1.3$, $\theta_s^d = 49\%$, $\theta_r^d = 8\%$) were deduced from McCartney and Zornberg (2010) using the van Genuchten–Mualem model (Equation 3). Considering that infiltration is a wetting process, drying WRC parameters were used to approximate the parameters of the wetting curve by following procedures proposed by Kool and Parker (1987) which were obtained after comparing measured drying and wetting water characteristic curves for different soils. In Kool and Parker's procedure, α^d is multiplied by two to obtain α^w in the wetting phase (i.e. $\alpha^w = 2\ \alpha^d$; where superscript d and w refers to main drying and wetting curves, respectively), while another parameter n remains the same. Thus, the fitting parameters for the wetting WRC of clay were determined as follows: $\alpha^w = 2 \times \alpha^d = 4.44\ kPa^{-1}$, $n^w = n^d = 1.3$, and $\theta_r^w = \theta_r^d = 8\%$. The effect of air entrapment in soil column was not considered in the simulation conducted in the current study, and it was assumed that fully saturated soil conditions could be achieved (i.e. $\theta_s^w = \theta_s^d = 49\%$). Figure 3 also shows a transition WRC measured by McCartney and Zornberg (2010) from a 125 mm high soil column (column B) with the same clay. The measured transition WRC is to justify the predicted wetting WRC.

McCartney and Zornberg (2010) obtained the dry- and wetting-path WRCs of geotextile physically by using a hanging column apparatus. Interestingly, a 75% volumetric moisture reduction in θ_s^w relative to θ_s^d was observed, indicating that a significant amount of air was entrapped in the geotextile (75% of voids were occupied by entrapped air) during wetting. The curve-fitting parameters of the wetting WRC of the geotextile ($\alpha^w = 5.0\ kPa^{-1}$, $n^w = 7.0$, $\theta_s^w = 24\%$, $\theta_r^w = 0\%$) were also determined using the van Genuchten–Mualem model. Since infiltration is a wetting process, wetting WRCs were used in the numerical simulation and to predict the hydraulic conductivity functions (k-functions) for the clay and geotextile.

The column was modelled using 5694 four-node quadrilateral elements with a global height of 0.01 m (Figure 4(b)). The nonwoven geotextile was modelled as

line elements. To ensure that the flow is only in the vertical direction, zero horizontal flux boundary conditions were set on both sides of the column. In this study, an automatically adjusted time increment between 1 and 100 s was selected as per requirement for attaining convergence. As suggested by Blake *et al.* (2003), the initial pore pressure was generated by applying a small prescribed unit flux at the top of the soil column model for a long period of time until steady-state conditions were reached. The values of the prescribed unit flux were adjusted until the calculated matrix suction distribution was close to and not exceeding the initial soil conditions in the physical model (i.e. $\theta_{initial} = 13.8\%$ and the corresponding $\psi_{initial} \approx 100$ kPa in this case). This is to ensure that the starting pore pressure head will not affect the generated pore water distribution in the subsequent transient seepage analyses. The importance of modelling an antecedent hydrology condition on any subsequent seepage modelling has been fully discussed by Blake *et al.* (2003).

To simulate infiltration, a $q = 3.4 \times 10^{-9}$ m/s for 3106 h was specified at the top. At the bottom of the column, to allow water to exit the column, the flux boundary condition was specified as $q = 0$ m/s and once the pore pressure became positive at any node on the bottom surface, the specified flux boundary condition was converted to the specified pressure-head boundary condition $h_p = 0$.

3.3. Comparison between numerical and experimental results

Figure 5(a) shows a comparison between the measured and predicted volumetric water content development at different elevations. As shown, for both the measured and predicted results, θ gradually increased because of the passing of the wetting front and the development of capillary barrier effect when the wetting front reached the soil–nonwoven geotextile interface. The development of the capillary barrier effect increased the water storage capacity of the soils beyond the limiting level that the soil could normally store under gravity. The predicted matric suctions corresponding to the change of θ with time were shown in Figure 5(b), which shows the predicted matric suctions decreased with the increase of θ with time.

In general, the numerical results showed a similar trend to the experimental results, suggesting that the numerical simulation could capture the capillary barrier effect well. The difference between the measured and predicted θ increased to approximately 5% at TDR4, the TDR near the GDL. This is likely to be because the effects of fine soil particle intrusion (clogging) into the geotextile during compaction and infiltration were not considered in the numerical simulation. Furthermore, the reduction of $k_{sat\ geotextile}$ due to air entrapment was not modelled. Iryo and Rowe (2004) reported that high soil moisture and pore pressure can be obtained above the geotextile by considering these effects. Despite the possible effects of soil clogging and air entrapment, the main objective of the numerical simulation (i.e. to validate the suitability of the developed numerical model for capturing the capillary barrier effect) could be achieved.

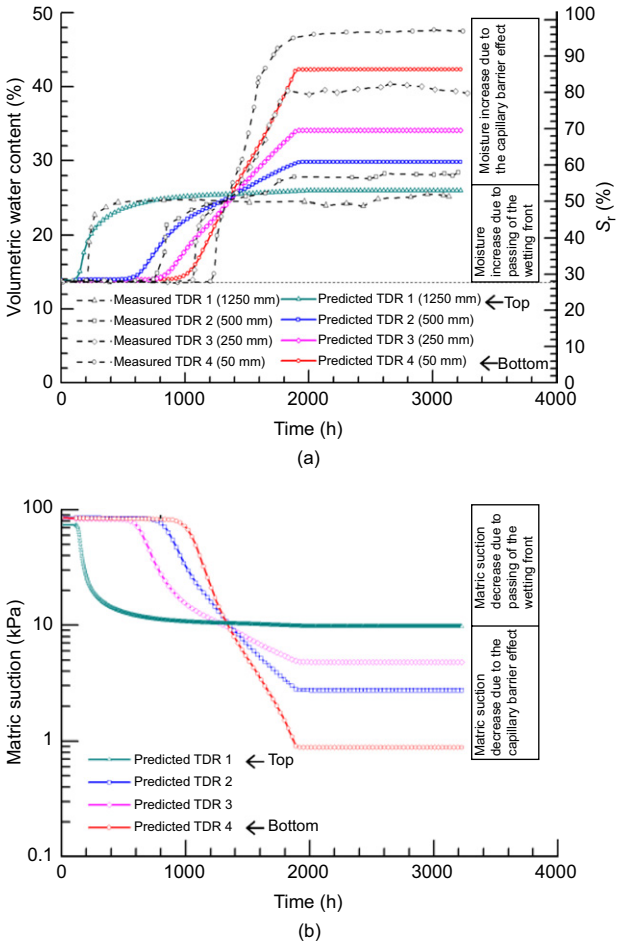

Figure 5. Moisture content and matric suction histories at different elevations (a) comparison of measured and predicted moisture content histories; (b) predicted matric suction histories (measured moisture content histories were adopted from McCartney and Zornberg (2010))

4. NUMERICAL ANALYSES OF INFILTRATION INTO UNSATURATED SLOPES

4.1. Model development and verification

4.1.1. *The experiment*

Iryo and Rowe (2005b) reported on the performance of full-scale embankment tests conducted by the Public Works Research Institute (PWRI), Japan. The embankments considered were 3 m high and 6 m long and had a slope of $0.7H:1V$ (= 55°), as shown in Figure 6(a). A series of finite-element simulations and a parametric study were conducted by Iryo and Rowe (2005b) to examine the effect of rainfall on the performance of the two slopes: one unreinforced (slope 1) and the other reinforced with nonwoven geotextile drains (slope 2).

Silty sand with 8% fine content was used as the backfill material. Figure 1 shows the grain size distribution and Table 1 summaries the hydraulic and shear strength properties of the backfill. Based on the gradation limits specified by design guidelines (Figure 1), the selected backfill material was on the boundaries of gradation limits between compliant and marginal soils. The backfill

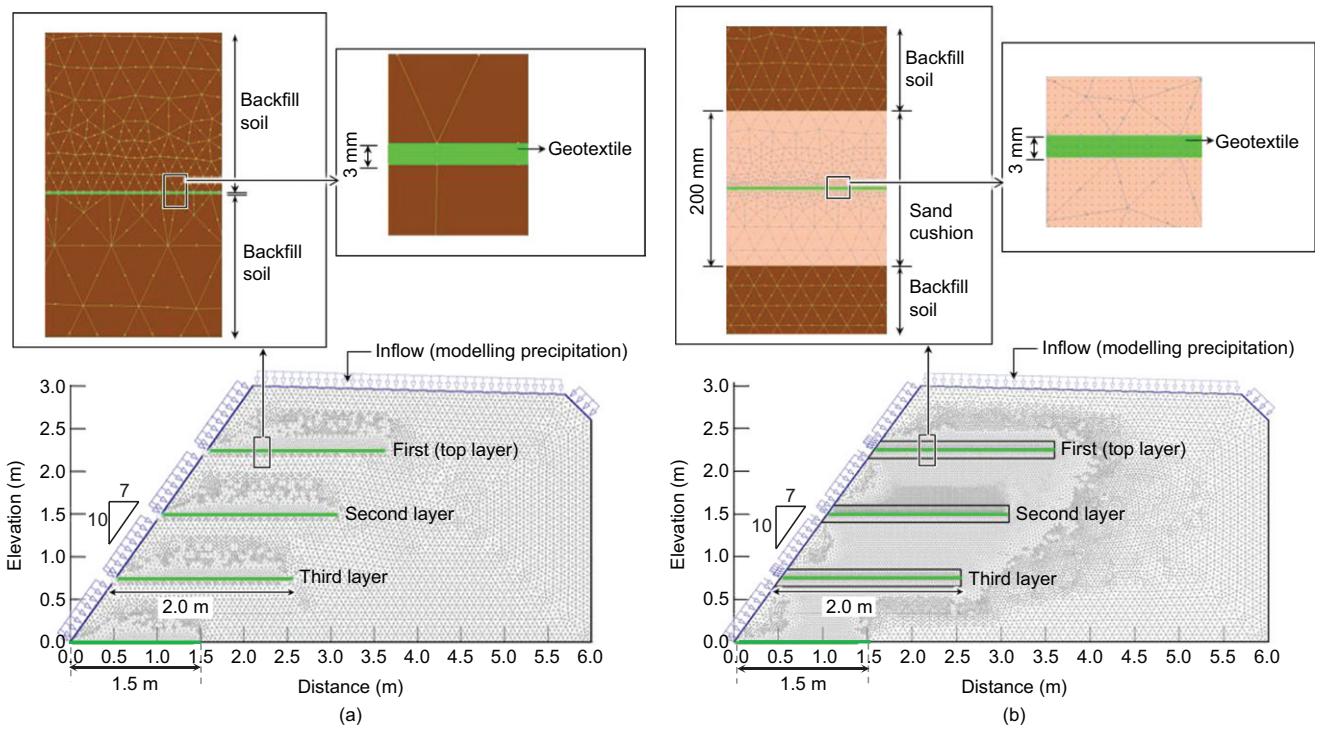

Figure 6. Typical infiltration model: (a) without sand cushion; (b) with geotextile sandwiched in sand cushion

had a gravimetric water content $\omega = 24\%$, and unit weight $\gamma_t = 17.5\ \text{kN/m}^3$. The saturated hydraulic conductivity was $k_{\text{sat backill}} = 1.3 \times 10^{-5}$ m/s. Four layers of nonwoven geotextile with a thickness of 3 mm for each layer were used as the drainage as well as the reinforcement material. The nonwoven geotextile had a mass per unit area of $310\ \text{g/m}^2$, porosity of 0.92, and saturated hydraulic conductivity of $k_{\text{sat geotextile}} = 2.3 \times 10^{-2}$ and 3.5×10^{-3} m/s in the in-plane and cross-plane directions, respectively. A 1.5 m long geotextile layer was placed at the toe of each embankment to prevent pore water pressures from developing at the base, and three layers of 2 m long nonwoven geotextile were placed with vertical spacings of 0.75 m within the backfill soil of the reinforced slope (Figure 6). Iryo and Rowe (2005b) reported that 10 cm of geotextile protruded above the slope surface. Therefore, the region 10 cm below each geotextile layer was shielded from infiltration.

After the slopes were constructed, artificial rainfall with an intensity of $q = 3.52 \times 10^{-6}$ m/s (=12.7 mm/h) was applied to the top and the sloping side of the slopes. During the experiment, the water content of the slopes was monitored using the radio isotope method along three vertical observation lines (1.2, 2.4, and 4.8 m from the toe). It was reported that the unreinforced slope (slope 1) failed first when the cumulative rainfall reached $R = 90$ mm (after 7.1 h). Slope 1 failed suddenly over the entire slope surface whereas slope 2 failed because of partial erosion on the slope surface. Erosion was initiated at a slope surface when the wetting front was stopped by the nonwoven geotextile layers, leading to the development of nearly saturated soil conditions within the soils immediately above the nonwoven geotextile.

4.1.2. *Numerical simulation*

In this study, two-dimensional models (Figure 6(a)) were developed by using SEEP/W software (Geo-Slope 2009). The slopes were modelled using 6445 six-node triangular elements arranged as shown in Figure 6(a). The global height of the elements was set to 0.1 m, constrained to a third of the global element size on top of the geotextile. To replicate the slopes constructed by the PWRI (described by Iryo and Rowe (2005b)), the base was considered to have a zero flux boundary, to simulate an impermeable solid concrete slab.

A $q = 3.52 \times 10^{-6}$ m/s ($= 0.27 k_{\text{sat soil}}$) was specified as the boundary condition on the top and side slope surfaces of both slopes 1 and 2 of the model for a period of 7.1 h. For simulating seepage from the embankment, once the pore pressure became positive at any node on the top surface and side slope surface, the boundary condition was changed from the specified flux boundary condition (i.e. infiltration rate) to a specified pressure-head condition ($h_p = 0$ m). An automatically adjusted time step increment between 1 and 100 s was selected for attaining convergence.

No information was provided on the unsaturated hydraulic properties of the soil used by the PWRI. Iryo and Rowe (2005b) obtained the van Genuchten–Mualem model parameters for the soil by considering typical published values and the parametric study results on the infiltration into the unreinforced slope. In this study, a drying WRC was first estimated from the soil particle size distribution using the method proposed by Fredlund *et al.* (1994). The estimated drying WRC was applied to deduce the drying curve fitting parameters (α^d, n^d, θ_s^d, θ_r^d) of the backfill soil using the van Genuchten–Mualem model. Thereafter, these drying parameters were used to

determine the wetting curve-fitting parameters (α^w, n^w, θ_s^w, θ_r^w) using the Kool and Parker's procedure (Kool and Parker 1987).

Figure 7 shows a comparison of the determined WRC and the results estimated by Iryo and Rowe (2005b). The WRC presented by Iryo and Rowe (2005b) appears to be the average of the drying and wetting WRCs determined in the present study. The nonwoven geotextile hydraulic characteristics used in this study agree with those determined by Iryo and Rowe (2005b); they obtained the hydraulic characteristics from the published physical properties of nonwoven geotextile with similar $k_{sat\ geotextile}$ and θ_s values. Figure 8 shows the hydraulic characteristics of the backfill soil and geotextile used in this study.

4.1.3. *Comparison between numerical and experimental results*

Figure 9 shows a comparison of the numerical and experimental degrees of saturation profiles and distribution contours for slopes 1 and 2. It can be observed that, in slope 2, the water content of the soils immediately above the geotextile layers is higher. Predictions related to the progress of the wetting front and moisture distributions within the slope during infiltration were consistent with experimental observations. The reason for the experimental results showing lesser variations in the S_r profiles can be attributed to the fact that the radio isotope method works on the basis of volume averaging principles, having limited resolution in water content measurements (Iryo and Rowe 2005b). A fair agreement between the numerical and experimental results suggests that the finite-element model is capable of modelling unsaturated seepage flow within soil slopes.

4.2. Numerical simulation program

After the numerical model was validated, numerical experiments were conducted to investigate the unsaturated hydraulic behaviour of soil slopes with nonwoven geotextile drains. In addition, the effect of sandwiching nonwoven geotextile drains in thin layers of sand was also investigated. Table 2 summarises the numerical simulations program. Each simulation case comprised three analyses: (1) infiltration at a specific infiltration rate; (2) overall stability analyses; and (3) local stability analyses.

A slope configuration presented previously was used (Figure 6). In cases where the nonwoven geotextile was sandwiched between sand cushions (Figure 6(b)), a 200 mm sand cushion was used to sandwich geotextile drains (100 mm on top and 100 mm at the bottom of the nonwoven geotextile). The fitting parameters of WRC of the sand cushion were adopted from Iryo and Rowe (2005a) but the saturated hydraulic conductivity was increased from 10^{-4} to 10^{-2} m/s to ensure a distinguish difference in the saturated hydraulic conductivity values between the selected backfill and sand cushion. The nonwoven geotextile reported by Iryo and Rowe (2004) (originally reported by Bathurst *et al.* (2007)) was selected in the numerical simulation program (slopes 3 and 4) to replace that used in the verification models (slope 2). The purpose is to achieve a clear increase in the pore water pressure due to the capillary barrier effect by using the nonwoven geotextile with lower permeability (the selected nonwoven geotextile had a $k_{sat\ geotextile}$ value approximately one order lower than that used in the verification

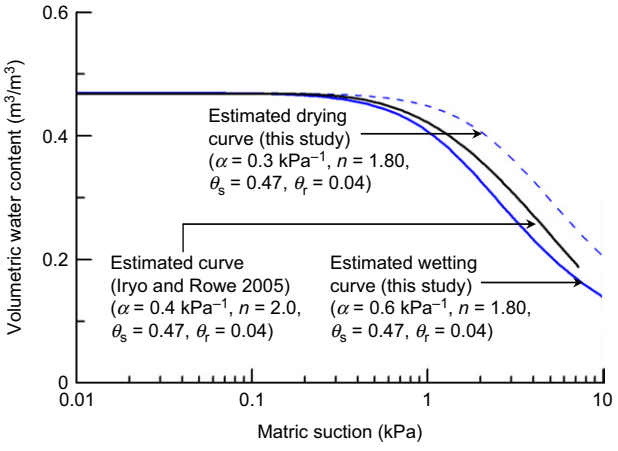

Figure 7. Comparison of estimated water retention curves of backfill soil

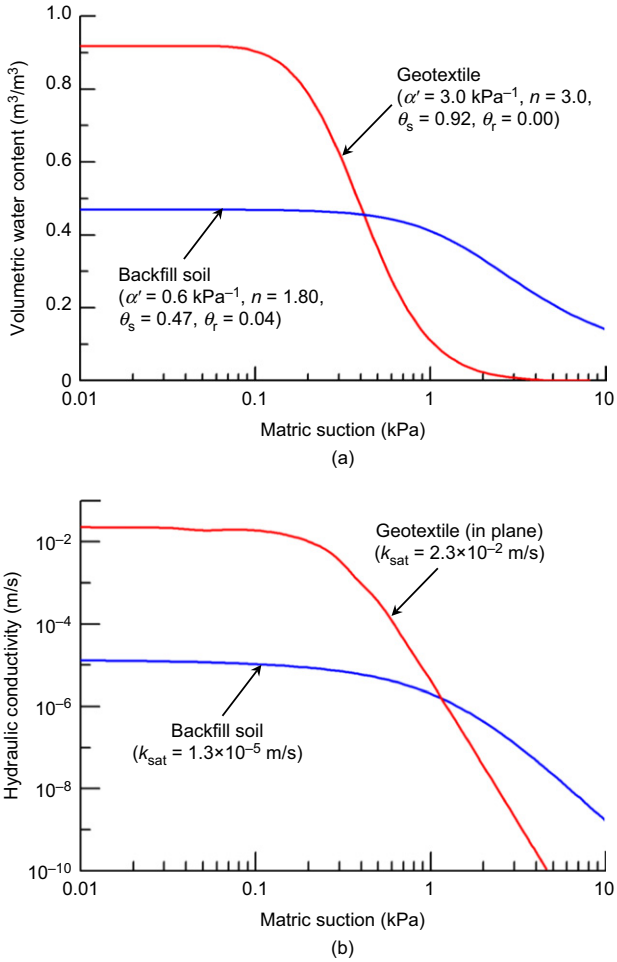

Figure 8. Material hydraulic characteristics used in slopes 1 and 2: (a) water retention curves; (b) hydraulic conductivity functions (WRC and *k*-function curve of nonwoven geotextile was adopted from Iryo and Rowe (2005b))

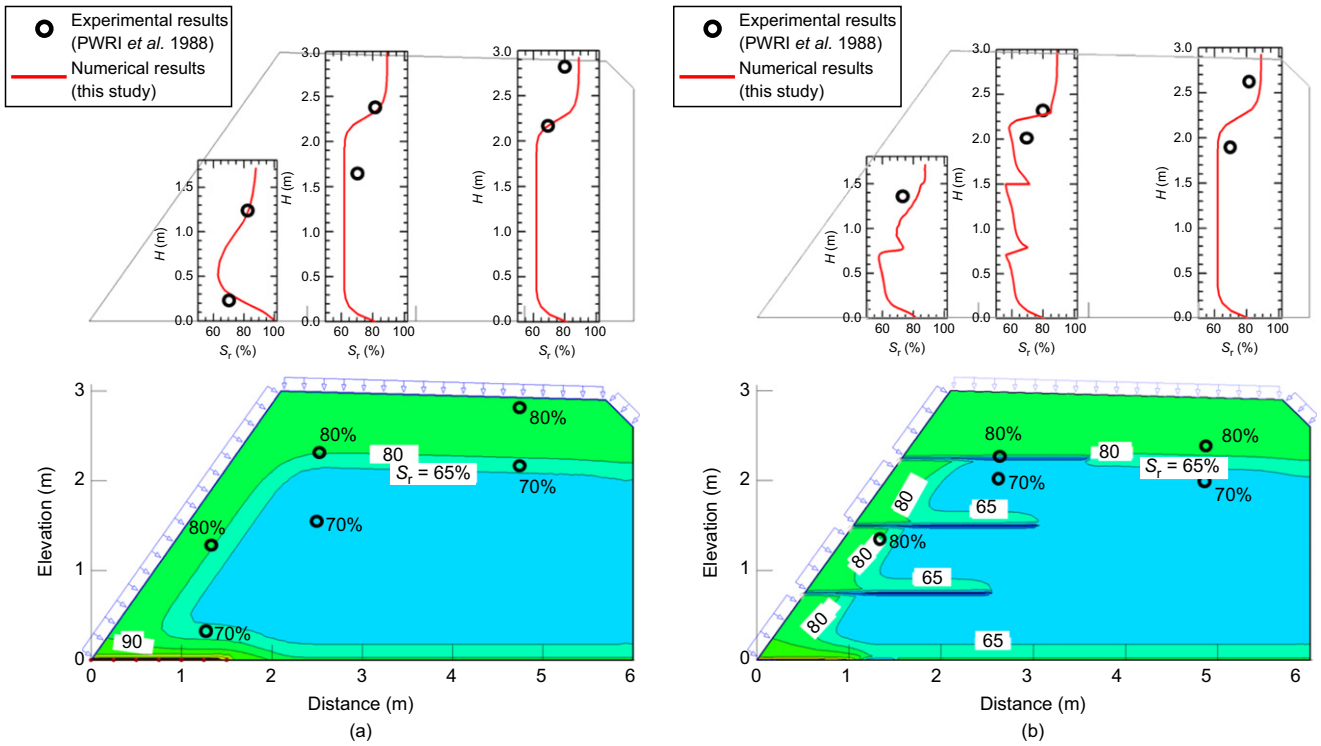

Figure 9. Numerical and experimental results of S_r profiles and distribution contours at $R = 90$ mm (after 7.1 h): (a) slope 1 (without geotextile drains); (b) slope 2 (with geotextile drains). Note: values inside white boxes indicate the predicted S_r results

models). Figure 10 shows the material hydraulic characteristics used for slopes 3 and 4.

Three infiltration conditions representing different rainfall intensities were used in each experiment. These conditions corresponded to infiltration boundary conditions for specified fluxes $q = 0.1k_{\text{sat backfill}}$ ($= 1.3 \times 10^{-6}$ m/s), $q = 0.5k_{\text{sat backfill}}$ ($= 6.5 \times 10^{-6}$ m/s) and for the specific pressure head $h_p = 0.1$ m (simulating the ponding case). The antecedent hydrology, as discussed earlier, was used to ensure that the initial condition was a uniform distribution of the pore pressure of −3.5 kPa. As the soil was placed with a controlled water content, this initial pore pressure value of −3.5 kPa was reported by Iryo and Rowe (2005b) based on the average value reported for all of the full-scale embankment tests.

To examine the effect of pore water increase resulting from the capillary barrier effect on the slope stability, limit-equilibrium-based slope stability analyses were conducted using the SLOPE/W software (Geo-Slope 2008). The overall factor of safety (FS) for the entire slope and the local FS for the soil above the top geotextile layer were analysed by applying the Spencer method for circular surfaces. The pore water pressures predicted by the SEEP/W software were used as the input pore pressures to calculate the soil effective stress. The unsaturated soil shear strength was determined using the modified Mohr–Coulomb failure criterion proposed by Fredlund *et al.* (1978).

$$\tau = c' + (\sigma - u_a)\tan\phi' + (u_a - u_w)\tan\phi^b \quad (5)$$

where τ is the unsaturated soil shear strength, c' is the effective cohesion of the saturated soil, ϕ' is the effective friction angle of the saturated soil, σ is the total stress on the failure plane, u_a is the pore air pressure, u_w is the pore water pressure, and ϕ^b is the friction angle indicating the rate of increase in shear strength relative to the matric suction. In this study, the backfill soil and sand cushions were modelled by considering $\gamma = 16.0$ kN/m^3, $\phi' = 40°$, $c' = 0$ kN/m^2, and $\phi^b = 16°$. The same soil property values were purposely selected for both backfill soil

Table 2. Numerical simulation program

Slope	Description	Infiltration condition		
		Case A $q = 0.1k_{\text{sat backfill}}$ (1.3×10^{-6} m/s)	Case B $q = 0.5k_{\text{sat backfill}}$ (6.5×10^{-6} m/s)	Case C $h_p = 0.1$ m (ponding case)
3	Backfill–nonwoven geotextile system	3-A	3-B	3-C
4	Backfill–sand cushion–nonwoven geotextile system	4-A	4-B	4-C

Note: slopes 1 and 2 are for model verification in Section 4.1.3.

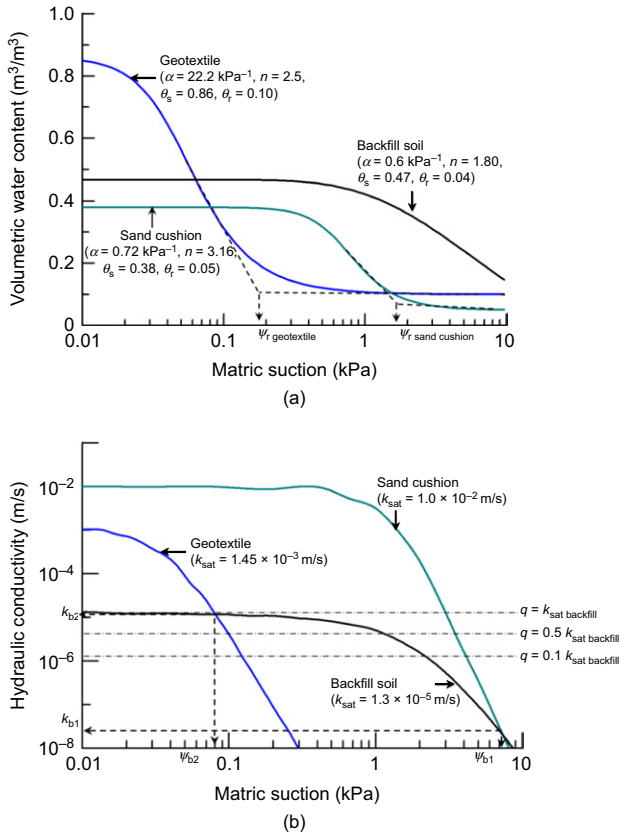

Figure 10. Hydraulic characteristics of material used in slopes 3 and 4: (a) water retention curve; (b) *k*-functions

and sand cushion with the intention of emphasising the difference in the calculated FS values caused solely by the capillary barrier effect rather than the effect of the difference in input soil shear strength properties. The tensile strength of the nonwoven geotextile was considered to be 20 kN/m according to the typical tensile strength range of geosynthetics reported by Shukla (2002) and Rowe (2001).

5. RESULTS AND DISCUSSION

5.1. Moisture and pore pressure profile

Figures 11 and 12 show the degree of saturation (S_r) contours and profiles, and pore water pressure profiles when the maximum pore pressure occurred above the first (top) geotextile layer (at time $t = 4.9$ h, with the corresponding accumulated rainfall $R = 115$ mm) in slopes 3-B (backfill–nonwoven geotextile system) and 4-B (backfill–sand cushion–nonwoven geotextile system). The pore pressure profiles in each geotextile layer in slope 3-B can be observed to be more discontinuous compared to those in slope 4-B. A positive pore water pressure developed in the top geotextile layer in slope 3-B, while the maximum pore water pressure in each geotextile layer remained negative in slope 4-B. These observations suggest that the capillary barrier effect developed in slope 3-B and that its effect was reduced by the inclusion of sand cushions. In slope 3-B, the capillary barrier effect momentarily led to restrictions on the water flow from the unsaturated backfill soil to the nonwoven geotextile. Consequently, the capillary barrier effect increased the water storage capacity of the soils above the nonwoven geotextile drain beyond the limiting level that they could normally retain under gravity.

In Figure 11(d), the seepage velocity vectors indicate that when the wetting front reached the soil–geotextile interface, water dispersion occurred in both (i.e. inward and outward) directions in the soil above the geotextile drain. The inward flow could also be caused by the advancing of the wetting front from the slope face, suggesting that inclining the drain toward the face of the slope would be helpful in guiding the dispersion of water out of the slope. The effect of geotextile inclination on the geotextile performance as a drainage layer has been evaluated by Iryo and Rowe (2005b). They suggested that geotextiles are more effective when they have an inclination of 10% under high infiltration. In Figure 12(d), the water entered the region within the upper and lower sand cushions, suggesting that the sand cushions also acted as additional drain layers to facilitate the drainage of water from the slope system.

Figures 13(b) and 14(b) show the development of pore pressure profiles in slopes 3-B and 4-B at a distance of 2.4 m from the toe, respectively. These profiles correspond to the instant at which the wetting front was halted and the maximum pore pressure developed above the top geotextile layer ($t = 17\,730$ s), second geotextile layer ($t = 35\,100$ s), and third geotextile layer ($t = 50\,940$ s). In slope 3-B, it can be observed that the pore water pressure increased in two steps: the initial increase occurring when the infiltration front passed through the soil layers and the subsequent increase being when the infiltration front was stopped by the nonwoven geotextile. When the wetting front infiltrated the soil layers, the pore pressures at the top of the slope increased to almost pressure levels corresponding to saturated conditions (i.e. −0.7 kPa), signifying a large loss of the matric suction from the original value of −3.5 kPa. Upon reaching the geotextile, the infiltration front was momentarily stopped, resulting in water accumulation and positive pore pressures (3.5 kPa) developing in the soils immediately above the top geotextile layer. In the soils below the geotextiles, the water migrated under gravity ($\psi < \psi_{initial}$) and was stopped by the lower geotextile layer. After the wetting front had passed through the geotextile layer, the developed positive pore pressures on top of the geotextile dropped and the pore pressure below the geotextile increased. The discontinuity in the pore pressure profiles decreased considerably after capillary breakthrough. Similar hydraulic behaviour was observed in the second and third geotextile layers when the wetting front reached these layers at $t = 35\,100$ and 50 940 s.

In slope 4-B, initially, when the wetting front infiltrated the soil layers, the pore pressures increased from −3.5 to 0.7 kPa at the top of the slope. This phenomenon was identical to what was observed in slope 3-B. However, in slope 4-B, when the infiltration front reached the first geotextile layer, the maximum pore pressures above the geotextile layer remained negative (−0.5 kPa) and the pore pressure profiles were less discontinuous at the

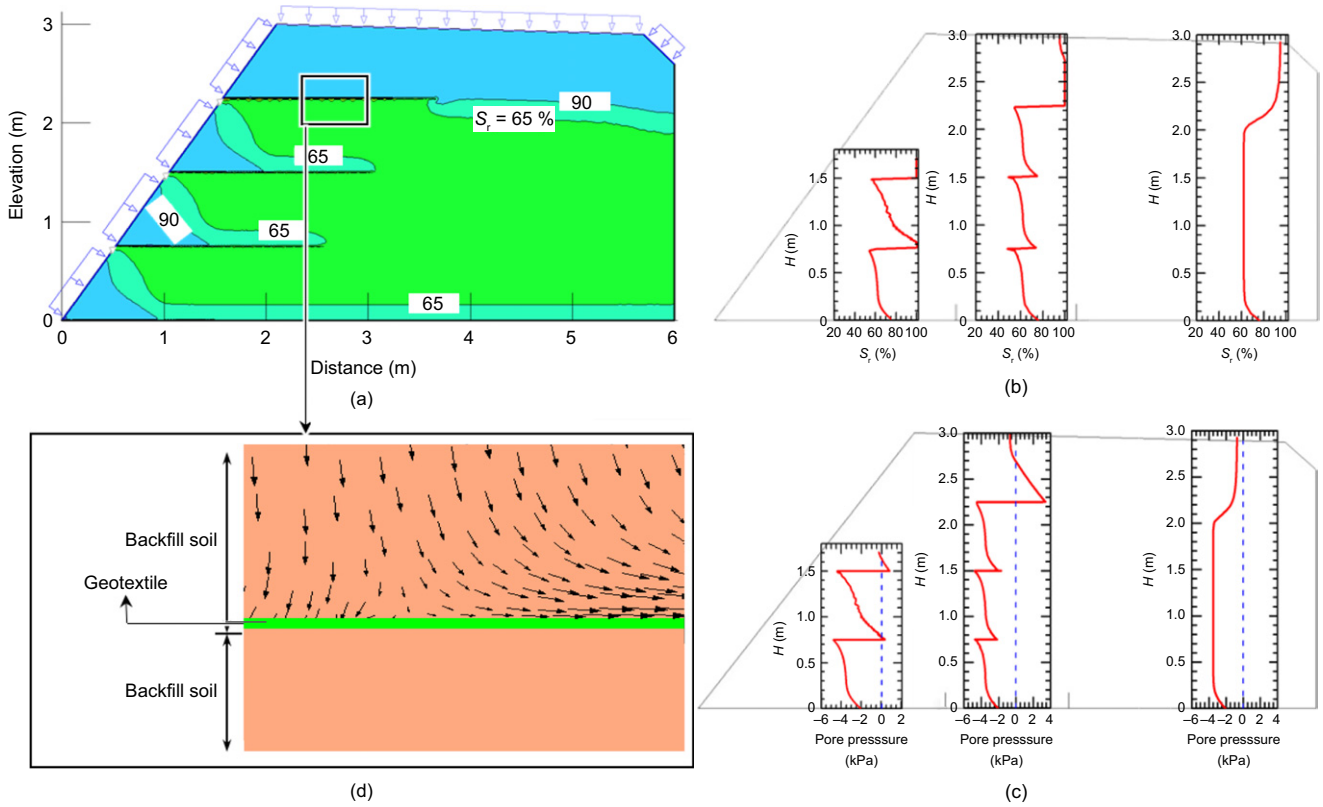

Figure 11. Advancing of infiltration when maximum pore pressure occurred above the top geotextile layer in slope 3-B (t = 4.9 h and the corresponding R = 115 mm): (a) S_r contours; (b) profiles of S_r; (c) pore pressure profiles; (d) seepage velocity

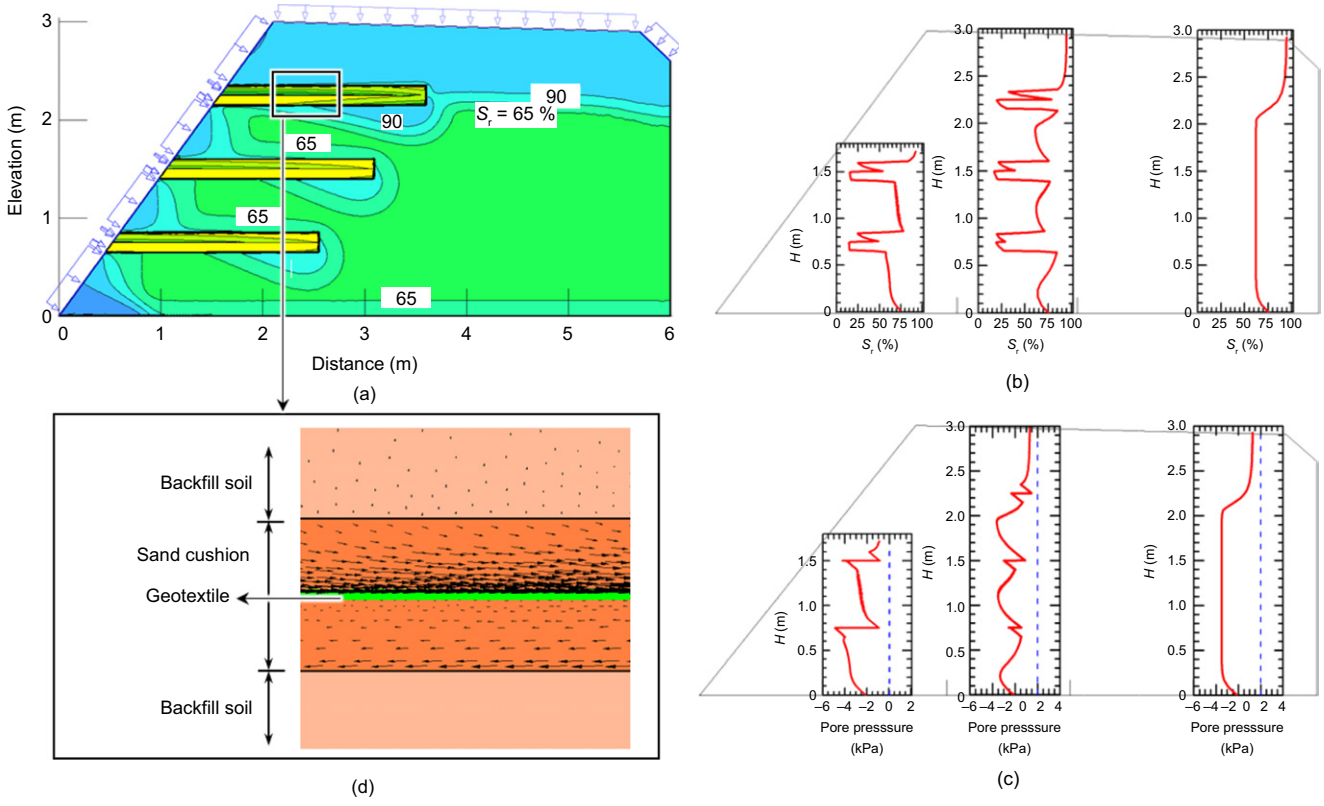

Figure 12. Advancing of infiltration when maximum pore pressure occurred above the top geotextile layer in slope 4-B (t = 4.9 h and the corresponding R = 115 mm): (a) S_r contours; (b) profiles of S_r; (c) pore pressure profiles; (d) seepage velocity vector

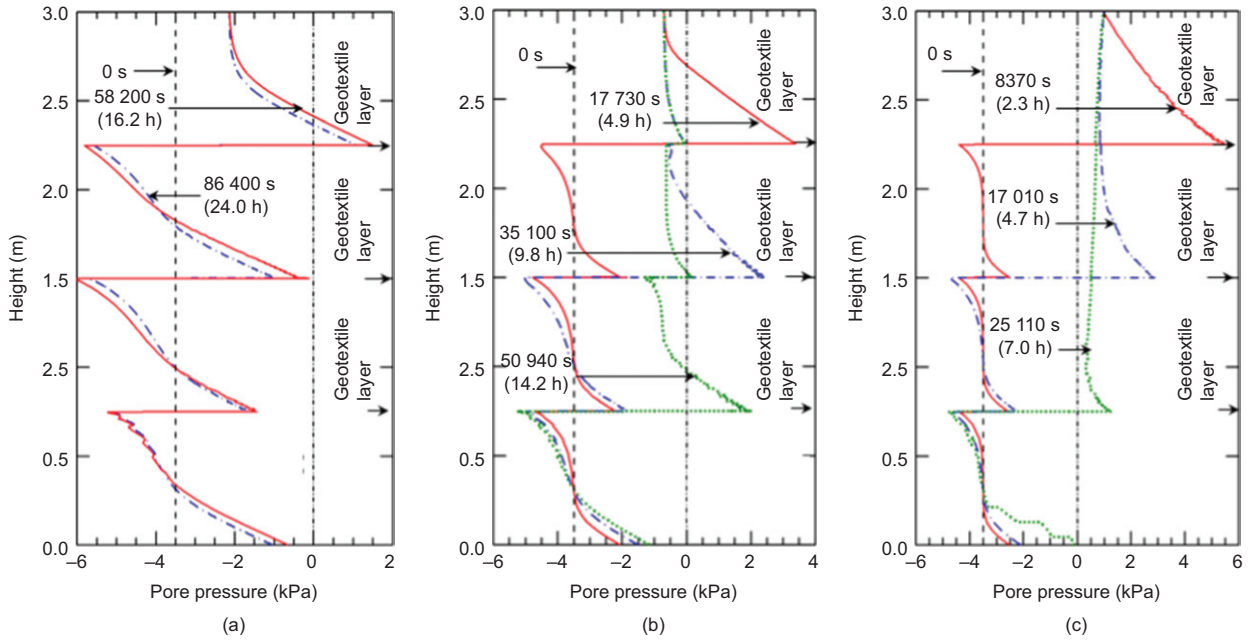

Figure 13. Development of pore pressure profiles at a distance of 2.4 m from the toe in slope 3 at different infiltration rates: (a) slope 3-A, $q = 0.1k_{\text{sat backfill}}$; (b) slope 3-B, $q = 0.5k_{\text{sat backfill}}$; (c) slope 3-C, $h_p = 0.1$ m (simulating ponding case)

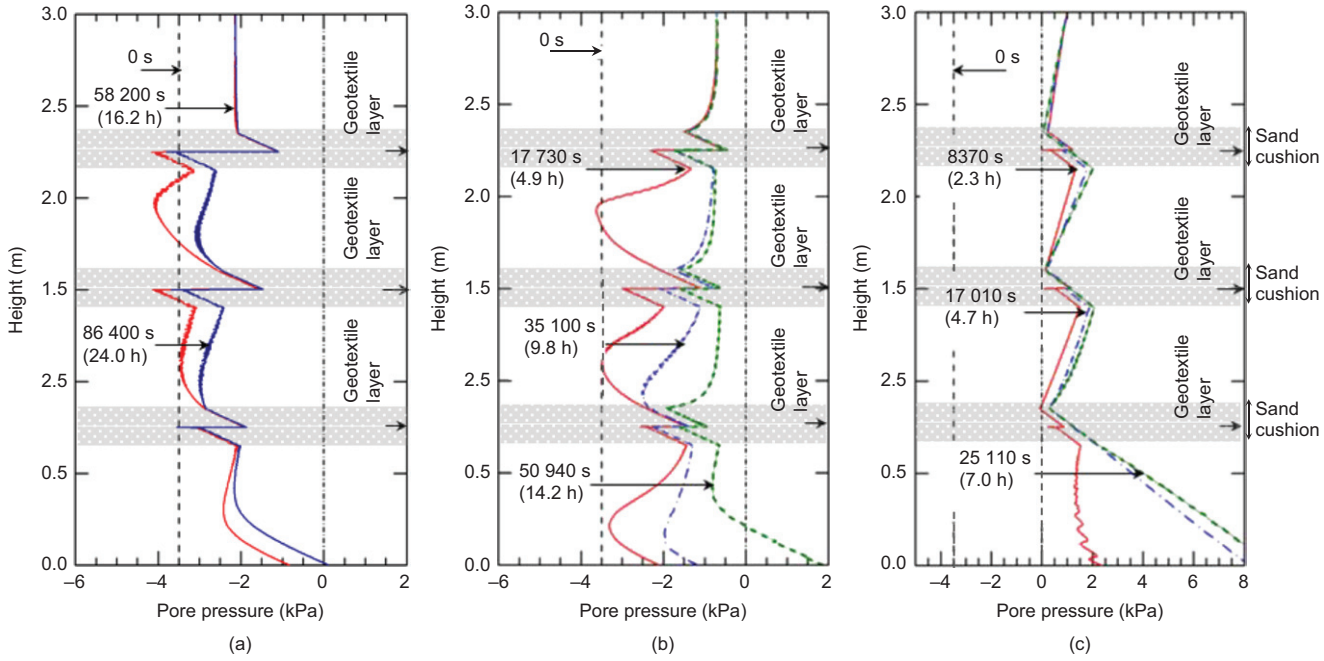

Figure 14. Development of pore pressure profiles at a distance of 2.4 m from the toe in slope 4 at different infiltration rates: (a) slope 4-A, $q = 0.1k_{\text{sat backfill}}$; (b) slope 4-B, $q = 0.5k_{\text{sat backfill}}$; (c) slope 4-C, $h_p = 0.1$ m (simulating ponding case)

soil–geotextile interface, compared to those of slope 3-B. Similar hydraulic behaviour was observed when the wetting front reached the second and third geotextile layers. The developing pore pressure remained negative above the second and third geotextile layers, suggesting that the inclusion of sand cushions in slope 4-B prevented the further development of pore water pressures.

The mechanism underlying the reduction in the capillary barrier effect when sand cushions are used can be explained as follows. The sand cushions acted as an intermediate material between the backfill and the nonwoven geotextile, which bridged the gap between two materials with contrasting unsaturated hydraulic characteristics. Thus, the use of the sand cushions reduced the amount of moisture accumulation required for the suction at the soil–geotextile interface to reach the critical value, thereby dissipating the accumulated pore water pressure within the soils above the geotextile downward effectively.

5.2. Overall and local stability

Figure 15 shows the variation of the overall and local FS values with R. In Figure 15(a), the overall FS values of

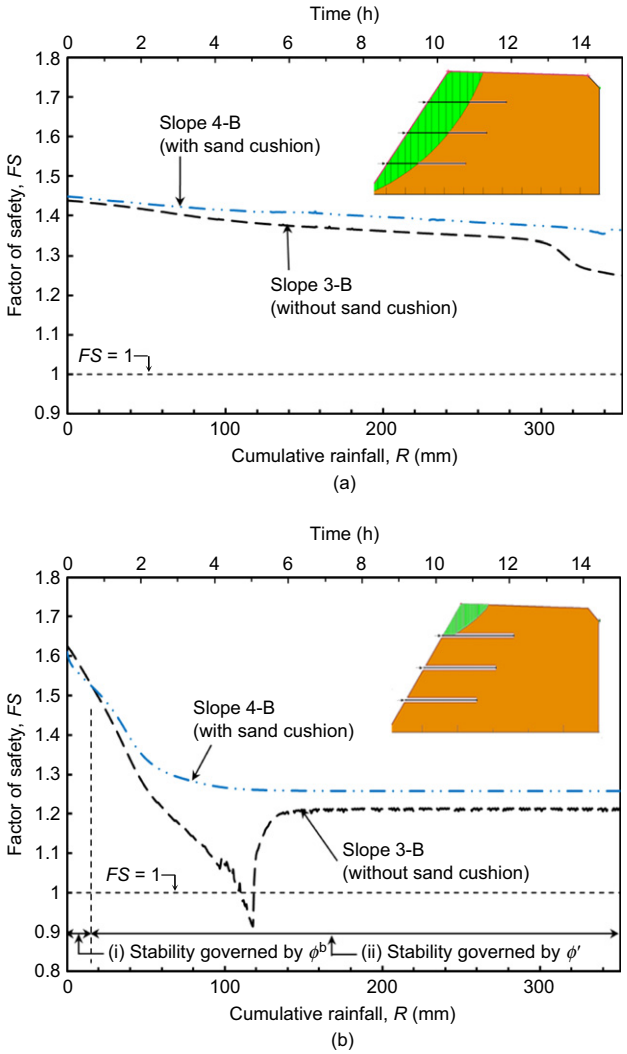

Figure 15. Variation of slope stability with cumulative rainfall for slopes 3-B and 4-B: (a) overall *FS*; (b) local *FS* for soils above the top geotextile layer

slopes 3-B and 4-B decrease with accumulated rainfall R. The overall FS of slope 4-B is slightly greater than that of slope 3-B at any given cumulative rainfall. The reason that the overall FS of slope 4-B was slightly greater than that of slope 3-B can be explained by comparing the variation of pore pressure along the failure surface for both cases (Figure 16). As the pore pressure along the failure surface was used in the limit equilibrium analysis to evaluate the slope stability (i.e. calculate FS), as shown in Figure 16; there was longer segments of failure surface in total having higher pore pressures in slope 3-B than in slope 4-B, specifically for higher positive pore water pressures at the location where each geotextile layer is intersected by the failure surface.

Figure 15(b) shows the local FS of slopes 3-B and 4-B for soils above the top geotextile layer. The local FS of slope 3-B at the beginning of infiltration in Section (i), which corresponds to the period when the system stability was governed by ϕ^b, was greater than that of slope 4-B. This is because at the beginning of infiltration, the backfill soil in both slopes was unsaturated; however, because of the relatively high hydraulic conductivity of the sand cushion (in slope 4-B), water ingress was considerably more rapid (water could also enter the slope from the slope face), and thus, the decrease in the matric suction in slope 4-B was subsequently relatively faster compared with slope 3-B, leading to a relatively lower FS in slope 4-B in the initial stage of infiltration. As infiltration continued, the matric suction decreased with increasing cumulative rainfall (in both slopes) and with the development of pore water pressure due to the capillary barrier effect in slope 3-B. Consequently, the local FS of slope 3-B decreased below that of slope 4-B when $R > 20$ mm in Section (ii), which corresponds to the period when the system stability was governed by ϕ'.

Interestingly, in Figure 15(b), at approximately $R = 120$ mm ($t = 4.9$ h), the local FS of slope 3-B reached the lowest value. This value was reached when the wetting

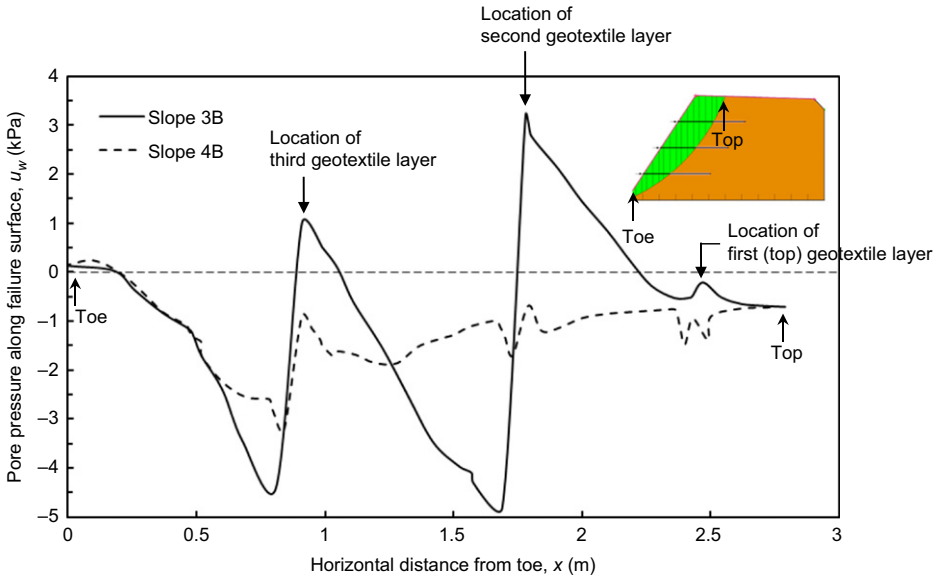

Figure 16. Variation of pore pressure along the failure surface for slopes 3-B and 4-B under $q = 0.5k_{sat\ backfill}$ at $t = 35\,100$ s (9.8 h)

front was momentarily held by the top geotextile layer due to the capillary barrier effect, and the development of the maximum pore pressure was observed (Figure 13(b)). After the wetting front had passed through the geotextile, the pore pressures on the top geotextile layer dissipated, leading to a significant increase in the FS in a short period. It was also observed that the FS of soils above the top geotextile layer in slope 3-B decreased below 1.0 (unstable condition), whereas that in slope 4-B was always above one. This indicates that local failure occurred due to the capillary barrier effect in slope 3-B. In this study, the computation of the FS was continued for FS < 1.0 (signifying slope failure) to demonstrate the recovery of the FS after capillary breakthrough.

In summary, sandwiching nonwoven geotextile drains between thin layers of highly draining sand can enhance the local and overall factor of safety by reducing the development of capillary barrier effect and improving the horizontal drainage capacity of the slope system.

5.3. Effect of infiltration rate

Figure 13 shows the development of pore pressure profiles at a distance of 2.4 m from the toe of slope 3 for different infiltration rates. At $q = 0.1k_{\text{sat backfill}}$ (slope 3-A in Figure 13(a)), the pore pressures at the top of slope increased from an initial value of −3.5 kPa to approximately −2.0 kPa. When the wetting front reached the top geotextile layer, pore pressures further increased to 1 kPa due to the capillary barrier effect. Since the infiltration rate was low, water accumulation took a long time and the numerical simulation of the infiltration process was completed at $t = 86\,400$ s (24 h), before the pore water pressure above the second geotextile layer reached the maximum value.

Figure 13(b) shows the developed pore pressure profiles in slope 3-B at $q = 0.5k_{\text{sat backfill}}$. As discussed previously, when the infiltration began, the pore pressures increased from −3.5 to −0.7 kPa at the top of the slope. When the wetting front reached the top geotextile layer, it was stopped due to the capillary barrier effect, and the pore water pressures increased to 3.5 kPa.

Figure 13(c) shows the developed pore pressure profiles in slope 3-C for the ponding case ($h_p = 0.1$ m). When the wetting front passed through the soils, the pore water pressures increased from −3.5 to 1 kPa at the top of the slope because of the effect of 0.1 m water ponding. Subsequently, when the wetting front reached the top geotextile layer, it was momentarily held due to the capillary barrier effect. The pore pressures increased up to 5.5 kPa.

Figure 13 also shows that q does not affect the occurrence of the capillary barrier effect; rather, it affects the maximum pore pressure above the geotextile layers associated with the capillary barrier effect and the pore pressure profile after capillary breakthrough (discussed in Section 5.4.1). Choo and Yanful (2000) found the water storage in a clay layer above the capillary barrier to be sensitive to the rate of infiltration. In addition, the geosynthetic capillary barrier can lead to an increase in θ up to a height of approximately 50–70 cm above the geotextile. The influenced height varies with q.

Figure 14 shows the development of pore pressure profiles at a distance of 2.4 m from the toe of slope 4 for different infiltration rates. The loss of matric suction at the top of the slope when the infiltration initiated was similar to that observed for slope 3 at any given infiltration rates. The main difference between infiltration into slopes 3 and 4 (from a comparison of Figures 13 and 14) was that when the wetting front reached the nonwoven geotextile layers, the inclusion of sand cushions in slope 4 reduced the capillary barrier effect and the maximum pore pressure in each geotextile layer remained negative, as shown in Figures 14(a) and 14(b). Although a small amount of water accumulated at the sand cushion–geotextile interface, the influenced height is much less than that at backfill–geotextile interface in slope 3 at a given q.

The magnitude of the capillary barrier effect is quantified by

$$\Delta u = u_{\text{soil–geotextile interface}} - u_{\text{top}} \tag{6}$$

where Δu is the pore pressure increase due to the capillary barrier effect, u_{top} is the pore pressure at the top of the slope when the infiltration began, corresponding to the condition in the soil layer in which there is no impact of the capillary barrier effect, and $u_{\text{soil–geotextile interface}}$ was the maximum pore pressure at the soil–nonwoven geotextile interface when the wetting front was stopped by the capillary barrier effect. Table 3 summarises the infiltration simulation results for various cases. As can be seen, both u_{top} and $u_{\text{soil–geotextile interface}}$ in slopes 3 and 4 increased with the infiltration rate. The Δu induced by the capillary barrier effect increased in slope 3 but decreased in slope 4 as the infiltration rate increased. In addition, Δu in slope 4

Table 3. Summary of infiltration simulation results

Slope	Initial pore pressure (kPa)	Maximum pore pressure within soils immediately above geotextile $u_{\text{soil-geotextile interface}}$ (kPa)			Pore pressure at the top of slope after wetting front passed u_{top} (kPa)			Pore pressure increase due to capillary barrier effect (Equation 6) Δu (kPa)		
		Case A $0.1k_{\text{sat backfill}}$	Case B $0.5k_{\text{sat backfill}}$	Case C 0.1 m	Case A $0.1k_{\text{sat backfill}}$	Case B $0.5k_{\text{sat backfill}}$	Case C 0.1 m	Case A $0.1k_{\text{sat backfill}}$	Case B $0.5k_{\text{sat backfill}}$	Case C 0.1 m
3	−3.5	1.5	3.5	5.5	−2	−0.7	1	3.5	4.2	6.5
4	−3.5	−1	−0.5	1	−2	−0.7	1	1	0.2	0

Note: values were determined when capillary barrier effect developed at the top of geotextile layer.

was less than that in slope 3 for various infiltration conditions. These observations suggest that the sand cushion effectively reduced the capillary barrier effect.

5.4. Discussion on occurrence of capillary barrier effect

The methods discussed in Section 2 were applied to examine the occurrence of the capillary barrier effect and to explain the pore water profiles after capillary breakthrough. The critical suction values (ψ_r and ψ_b), as discussed in Section 2, are indicated in the WRC and k-functions in Figure 10. The suction at which the hydraulic conductivity curve of the backfill soil intersects the hydraulic conductivity curve of the sand cushion is denoted by ψ_{b1} and the corresponding hydraulic conductivity rate is represented by k_{b1}. Furthermore, subscript 2 refers to the point at which the hydraulic conductivity curve of the backfill soil intersects the hydraulic conductivity curve of the geotextile (i.e. ψ_{b2} and k_{b2}).

5.4.1. *Discussion on slope 3*

As discussed in Section 2, the capillary barrier effect occurs in the soil–geotextile system when $\psi_{initial} > \min(\psi_{r\ geotextile}, \psi_b)$. For the materials in slope 3 (Figure 10), the following are the parameter values: $\psi_{initial} = 3.5$ kPa, $\psi_{r\ geotextile} = 0.15$ kPa, and $\psi_{b2} = 0.08$ kPa ($\psi_{b2} < \psi_{r\ geotextile} < \psi_{initial}$). This indicates that water could freely enter the geotextile at a matric suction of 0.15 kPa, but only at a very small rate until the matric suction reached $\psi_{b2} = 0.08$ kPa, when the flow rate changed to that matching the hydraulic conductivity of the geotextile at the corresponding suction. Consequently, the capillary barrier effect occurred in all infiltration simulations performed for slope 3, as shown in Figure 13.

It was also observed that the infiltration rate influenced the pore water pressure profiles after the wetting front passed through the geotextile. In slopes 3-A and 3-B ($q < k_{sat\ backfill}$), after capillary breakthrough, the pore pressures in the soil *below* the geotextile layer increased but did not become positive because q was smaller than the outflow flux ($\approx k_{sat\ backfill}$). The capillary barrier did not completely disappear after the wetting front broke through the geotextile, a pore pressure discontinuity remained above the geotextile (Figure 13(b)). In slope 3-C ($q \approx k_{sat\ backfill}$), the discontinuity in the pore water pressure was not observed after the wetting front passed through the geotextile layer (the Δu is fully dissipated in Figure 13(c)) because the geotextile became more permeable than the soil when it was saturated. The aforementioned observations support the statements of Iryo and Rowe (2004, 2005a) presented in Section 2.

5.4.2. *Discussion on slope 4*

For the sand cushions in slope 4 (Figure 10), the following are the parameter values: $\psi_{initial} = 3.5$ kPa, $\psi_{r\ sand\ cushion} = 1.5$ kPa, and $\psi_{b1} = 7$ kPa ($\psi_{r\ sand\ cushion} < \psi_{initial} < \psi_{b1}$). At the backfill-sand cushion interface, the hydraulic conductivity of the sand cushion was higher than that of the backfill material at $\psi_{b1} < 7$ kPa; however, water could not flow into the sand cushion until $\psi_{r\ sand\ cushion} = 1.5$ kPa. The initial matric suction in the backfill soil and sand cushion was 3.5 kPa (less than ψ_{b1}), implying that when $\psi_{r\ sand\ cushion}$ reached 1.5 kPa, the wetting front quickly dissipated in the sand cushion because the hydraulic conductivity of the sand cushion was higher than that of the backfill material. Therefore, the capillary barrier effect could not occur at the backfill–sand cushion interface (Figure 14) for $\psi < 1.5$ kPa. Compared the critical suction threshold $\psi = 1.5$ kPa for slope 4 with $\psi = 0.08$ kPa for backfill soil–geotextile interface in slope 3, the sand cushion acted as an intermediate material between the backfill and nonwoven geotextile, reducing the stored moisture required for attaining the critical suction value at the soil–geotextile interface.

When the suction decreased to $\psi_{r\ geotextile} = 0.15$ kPa at the sand cushion–geotextile interface, the wetting front started to enter the nonwoven geotextile. A capillary barrier effect would be expected to occur because the hydraulic conductivity of the geotextile was lower than that of the sand cushion. However, this interface is considered a relatively brittle capillary barrier because of the high hydraulic conductivity of the sand cushion once the water has broken through from the backfill. As a result, as shown in Figure 14, only a small amount of water has accumulated at the sand cushion-geotextile interface and the pore water pressure did not increase to positive values in slope 4-A and 4-B.

6. CONCLUSIONS

A series of numerical analyses were conducted to investigate the hydraulic behaviour of unsaturated slopes with nonwoven geotextile drains. The effect of sand cushions on reducing the development of the capillary barrier effect was evaluated and discussed. The conclusions drawn from this study are summarised below.

- The suitability of the numerical model for modelling the capillary barrier effect and flow within unsaturated soils was validated by using the experimental results of a one-dimensional soil column infiltration test and full-scale infiltration tests.
- For the slope with nonwoven geotextile drains without sand cushions (slope 3), the numerical results indicated that the wetting front was momentarily stopped due to the capillary barrier effect at the interface between the soil and the underlying geotextile, and positive pore pressures developed in the soils immediately above the geotextile. An apparent discontinuity in the pore pressures was observed above and below the geotextile layer. In this case, the nonwoven geotextile acted as a moisture barrier instead of acting as a drainage material.
- The capillary barrier effect was appreciably reduced by sandwiching geotextile drains between suitable sand cushions (slope 4). The maximum pore water pressure in soils above each geotextile layer remained negative, and the pore pressure profiles were less discontinuous compared to those of slope 3. In this case, sand cushions acted as an intermediate material

between the backfill and the nonwoven geotextile, which bridged the gap between two materials with contrasting unsaturated hydraulic characteristics; consequently, the pore water pressure in the soils above the nonwoven geotextile was effectively dissipated downward.

- The overall and local slope stabilities were evaluated by considering pore pressure changes in each infiltration stage. As infiltration continued, local soil failure occurred for soils above the top geotextile layer because of the development of positive pore water pressure, induced by the capillary barrier effect. The use of sand cushions enhanced both overall and local slope stabilities.
- Numerical results indicated that the capillary barrier effect occurred irrespective of the infiltration rate. However, the infiltration rate influenced not only the pore water pressure increase Δu induced by the capillary barrier effect but also the pore pressure profile after capillary breakthrough. The pore pressure increase Δu for slope 4 was lower than that for slope 3 for various infiltration conditions, suggesting that the sand cushions effectively reduced the capillary barrier effect.

For the application of geosynthetic drains in reinforced structures with marginal backfill soils, the designer should be aware of the possibility of capillary barrier effect occurring. The relationship among the hydraulic characteristics of the unsaturated soil and geotextile and the infiltration rate can be used to select suitable nonwoven geotextile and sand cushions for a particular backfill to prevent or reduce the capillary barrier effect. Finally, this study demonstrated the effectiveness of the use of sand cushions. The type, thickness, and coverage area of the sand cushions may play an important role in determining the efficiency with which the capillary barrier effect is reduced, and therefore, they should be further investigated.

ACKNOWLEDGEMENTS

The financial support for this research was from the Ministry of Science and Technology of Taiwan under grant no. NSC102-2221-E-011-057-MY3. The financial support for the first author was provided by the Ministry of Education of Taiwan under the grant for 'Aim for the Top-Tier University Project'. These financial supports are gratefully acknowledged.

NOTATION

Basic SI units are given in parentheses.

c' effective cohesion of saturated soil (Pa)
$\boldsymbol{g}$ gravity (m/s^2)
h total hydraulic head (m)
h_p pressure head (m)
k hydraulic conductivity (m/s)
k_b hydraulic conductivity at which hydraulic conductivity functions of two materials forming interface intersect (m/s)
k_{b1} hydraulic conductivity at which the hydraulic conductivity curve of backfill soil intersects the hydraulic conductivity curve of sand cushion (m/s)
k_{b2} hydraulic conductivity at which the hydraulic conductivity curve of backfill soil intersects the hydraulic conductivity curve of geotextile (m/s)
k_{sat} saturated hydraulic conductivity (m/s)
$k_{sat\ backfill}$ saturated hydraulic conductivity of backfill soil (m/s)
$k_{sat\ geotextile}$ saturated hydraulic conductivity of geotextile (m/s)
$k_{sat\ soil}$ hydraulic conductivity of soil (m/s)
k_x hydraulic conductivity in x-direction (m/s)
k_y hydraulic conductivity in y-direction (m/s)
m fitting parameter for van Genuchten equations (dimensionless)
m_w coefficient of water volume change (dimensionless)
n fitting parameter for van Genuchten equations (dimensionless)
n^d fitting parameter for van Genuchten equations for drying curve (dimensionless)
n^w fitting parameter for van Genuchten equations for wetting curve (dimensionless)
q infiltration rate/boundary flux (m/s)
R cumulative rainfall (m)
S_r degree of saturation (dimensionless)
t time (s)
u_a pore air pressure (Pa)
$u_{soil–geotextile\ interface}$ maximum pore pressure at the soil–geotextile interface (Pa)
u_{top} pore pressure at the top of slope (Pa)
u_w pore water pressure (Pa)
α fitting parameter for van Genuchten equations (Pa^{-1})
α^d fitting parameter for van Genuchten equations on drying curve (Pa^{-1})
α^w fitting parameter for van Genuchten equations on wetting curve (Pa^{-1})

Δu pore pressure increment due to capillary barrier effect (Pa)
ϕ' effective friction angle (°)
ϕ^b friction angle indicating the rate of increase in shear strength relative to matric suction (°)
γ unit weight of soil (N/m^3)
γ_w unit weight of water (N/m^3)
Θ normalised volumetric water content (dimensionless)
θ volumetric water content (dimensionless)
θ_r^d residual volumetric water content for drying curve (dimensionless)
θ_s^d saturated volumetric water content for drying curve (dimensionless)
θ_r residual volumetric water content (dimensionless)
θ_s saturated volumetric water content (dimensionless)
θ_r^w residual volumetric water content for wetting curve (dimensionless)
θ_s^w saturated volumetric water content for wetting curve (dimensionless)
ρ_w density of water (kg/m^3)
σ total stress along the failure plane (Pa)
τ soil shear strength (Pa)
ω gravimetric water content (dimensionless)
ψ matric suction (Pa)
ψ_b suction at which hydraulic conductivity functions of two materials forming interface intersect (Pa)
ψ_{b1} suction at which the hydraulic conductivity curve of backfill soil intersects the hydraulic conductivity curve of sand cushion (Pa)
ψ_{b2} suction at which the hydraulic conductivity curve of backfill soil intersects the hydraulic conductivity curve of geotextile (Pa)
$\psi_{initial}$ initial matric suction (Pa)
ψ_r residual matric suction (Pa)
$\psi_{r\ geotextile}$ residual matric suction of geotextile (Pa)
$\psi_{r\ sand\ cushion}$ residual matric suction of sand cushion (Pa)

REFERENCES

AASHTO (2002). *Standard Specifications for Highway Bridges*, 17th edn. American Association of State Highway and Transportation Officials, Washington, DC, USA.

Abdi, M. R. & Zandieh, A. R. (2014). Experimental and numerical analysis of large scale pull out tests conducted on clays reinforced with geogrids encapsulated with coarse material. *Geotextiles and Geomembranes*, **42**, No. 5, 494–504.

Abdi, M. R., Sadrnejad, A. & Arjomand, M. A. (2009). Strength enhancement of clay by encapsulating geogrids in thin layers of sand. *Geotextiles and Geomembranes*, **27**, No. 6, 447–455.

ASTM D698 *Standard Test Methods for Laboratory Compaction Characteristics of Soil using Standard Effort*. ASTM International, West Conshohocken, PA, USA.

ASTM D2487 *Standard Practice for Classification of Soils for Engineering Purposes (Unified Soil Classification System)*. ASTM International, West Conshohocken, PA, USA.

Azevedo, M. & Zornberg, J. G. (2013). Capillary barrier dissipation by new wicking geotextile. *Panamerican Conference on Unsaturated Soils*, 20–22 February, Cartagena de Indias, Colombia, pp. 559–565.

Bathurst, R. J., Ho, A. F. & Siemens, G. (2007). A column apparatus for investigation of 1-D unsaturated saturated repsone of sand-geotextile systems. *Geotechnical Testing Journal*, **30**, No. 6, 1–9.

Bathurst, R. J., Siemens, G. & Ho, A. F. (2009). Experimental investigation of infiltration ponding in one-dimensional sand–geotextile columns. *Geosynthetics International*, **16**, No. 3, 158–172.

Berg, R., Christopher, B. R. & Samtani, N. (2009). *Design of Mechanically Stabilized Earth Walls and Reinforced Soil Slopes*, Report No. FHWA-NHI-10-024, vol. I and II. National Highway Institute, Federal Highway Administration, Washington, DC, USA.

Blake, J. R., Renaud, J. P., Anderson, M. G. & Hencher, S. R. (2003). Prediction of rainfall-induced transient water pressure head behind a retaining wall using a high-resolution finite element model. *Computers and Geotechnics*, **30**, No. 6, 431–442.

Bouazza, A., Zornberg, J. G., McCartney, J. & Singh, R. (2013). Unsaturated geotechnics applied to geoenvironmental engineering problems involving geosynthetics. *Engineering Geology*, **165**, 143–153.

Choo, L. P. & Yanful, E. K. (2000). Water flow through cover soils using modeling and experimental methods. *Journal of Geotechnical and GeoEnvironmental Engineering*, **126**, No. 4, 324–334.

Christopher, B. R. & Stuglis, R. S. (2005). Low permeable backfill soils in geosynthetics reinforced soil wall: state of the practice in North America. *Proceedings of North American Geo-synthetics Conference (NAGS 2005)*, Las Vegas, NV, USA, GRI-19, p. 14e16.

Christopher, B. R., Zornberg, J. G. & Mitchell, J. K. (1998). Design guidance for reinforced soil structures with marginal soil backfills. *Proceedings of the 6th International Conference on Geosynthetics*, Atlanta, GA, USA, vol. 2, pp. 797–804.

Elias, V., Christopher, B. R. & Berg, R. (2001). *Mechanically Stabilized Earth Walls and Reinforced Soil Slopes Design and Construction Guidelines*, Report No. FHWA-NHI-00-043. National Highway Institute, Federal Highway Administration, Washington, DC, USA.

Fredlund, D. G. (2006). Unsaturated soil mechanics in engineering practice. *Journal of Geotechnical and Geoenvironmental Engineering*, **132**, No. 3, 286–321.

Fredlund, D. G., Morgenstern, N. R. & Widger, A. (1978). Shear strength of unsaturated soils. *Canadian Geotechnical Journal*, **15**, No. 3, 313–321.

Fredlund, D. G., Xing, A. Q. & Huang, S. (1994). Predicting the permeability functions for unsaturated soils using the soil-water characteristics curve. *Canadian Geotechnical Journal*, **31**, No. 3, 521–532.

Garcia, E. F., Gallage, C. P. K. & Uchimura, T. (2007). Function of permeable geosynthetics in unsaturated embankment subjected to rainfall infiltration. *Geosynthetics International*, **14**, No. 2, 89–99.

Geo-Slope (2008). *Stability Modeling with SLOPE/W*, GEO-SLOPE International Ltd, Calgary, Canada.

Geo-Slope (2009). *Seepage Modeling with SEEP/W 2007*, GEO-SLOPE International Ltd, Calgary, Canada.

Huang, C. C. & Lo, C. L. (2013). Simulation of subsurface flows associated with rainfall-induced shallow slope failures. *Journal of GeoEngineering*, **8**, No. 3, 101–111.

Huang, C. C., Lo, C. L., Jang, J. S. & Hwu, L. K. (2008). Internal soil moisture response to rainfall-induced slope failures and debris discharge. *Engineering Geology*, **101**, No. 3–4, 134–145.

Iryo, T. & Rowe, R. K. (2003). On the hydraulic behavior of unsaturate nonwoven geotextiles. *Geotextiles and Geomembranes*, **21**, No. 6, 381–404.

Iryo, T. & Rowe, R. K. (2004). Numerical study of infiltration into a soil-geotextile column. *Geosynthetics International*, **11**, No. 2, 377–389.

Iryo, T. & Rowe, R. K. (2005a). Hydraulic behaviour of soil-geocomposite layers in slopes. *Geosynthetics International*, **12**, No. 3, 145–155.

Iryo, T. & Rowe, R. K. (2005b). Infiltration into an embankment reinforced by nonwoven geotextiles. *Canadian Geotechnical Journal*, **42**, No. 2, 1145–1159.

Koerner, R. M. & Koerner, G. R. (2013). A data base statistics and recommendations regarding 171 failed geosynthetic reinforced mechanically stabilized earth (MSE) walls. *Geotextiles and Geomembranes*, **40**, 20–27.

Kool, J. B. & Parker, J. C. (1987). Development and evaluation of closed form expression for hysteris soil hydraulic properties. *Water Resources Research*, **23**, No. 1, 105–114.

Lin, C. Y. & Yang, K. H. (2014). Experimental study on measures for improving the drainage efficiency of low-permeability and low-plasticity silt with nonwoven geotextile drains. *Journal of the Chinese Institute of Civil and Hydraulic Engineering*, **26**, No. 2, 71–82 (in Chinese).

Liu, C. N., Yang, K. H., Ho, Y. H. & Chang, C. M. (2012). Lessons learned from three failures on a high steep geogrid-reinforced slope. *Geotextiles and Geomembranes*, **34**, No. 3, 131–143.

Mancarella, D., Doglioni, A. & Simeone, V. (2012). On capillary barrier effffects and debris slide triggering in unsaturated layered covers. *Engineering Geology*, **147–148**, 14–27.

McCartney, J. S. & Zornberg, J. G. (2010). Effects of infiltration and evaporation on geosynthetic capillary barrier performance. *Canadian Geotechnical Journal*, **47**, No. 11, 1201–1213.

McKean, J. & Inouye, K. (2001). Field evaluation of the long-term performance of geocomposite sheet drains. *Geotextiles and Geomembranes*, **19**, No. 4, 213–234.

Mitchell, J. K. & Zornberg, J. G. (1995). Reinforced soil structures with poorly draining backfills. Part II: case histories and applications. *Geosynthetics International*, **2**, No. 1, 265–307.

NCMA (National Concrete Masonry Association) (2010). *Design Manual for Segmental Retaining Walls*, 3rd edn, National Concrete Masonry Association, Herndon, VA, USA.

Raisinghani, D. V. & Viswanadham, B. V. S. (2010). Evaluation of permeability characteristics of a geosynthetic-reinforced soil through laboratory tests. *Geotextiles and Geomembranes*, **28**, No. 6, 579–588.

Raisinghani, D. V. & Viswanadham, B. V. S. (2011). Centrifuge model study on low permeable slope reinforced by hybrid geosynthetics. *Geotextiles and Geomembranes*, **29**, No. 1, 567–580.

Richards, L. A. (1931). Capillary conduction of liquids through porous mediums. *Physics*, **1**, No. 5, 318–333.

Richardson, G. N. (1997). Fundamental mistakes in slope design. *Geotechnical Fabrics Report*, **15**, No. 2, 15–17.

Rowe, R. K. (2001). *Geotechnical and Geoenvironmental Engineering Handbook*, Kluwer Academic Publishing, Norwell, MA, USA.

Santos, E. C. G., Palmeira, E. M. & Bathurst, R. J. (2014). Performance of two geosynthetic reinforced walls with recycled construction waste backfill and constructed on collapsible ground. *Geosynthetics International*, **21**, No. 4, 256–269.

Shukla, S. K. (2002). *Geosynthetics and Their Applications*, Thomas Telford Publishing, London, UK, p. 430.

Siemens, G. & Bathurst, R. J. (2010). Numerical parametric investigation of infiltration in one-dimnesional sand-geotextile columns. *Geotextiles and Geomembranes*, **28**, No. 5, 460–474.

Stormont, J. C. & Morris, C. E. (2000). Characterization of unsaturated nonwoven geotextiles. *Advances in Unsaturated Geotechnics*, Shackelford, C. D., Houstoun, S. L. & Chang, N. Y., Editors, ASCE, Reston, VA, USA, pp. 153–164.

Unnikrishnan, N., Rajagopal, K. & Krishnaswamy, N. R. (2002). Behaviour of reinforced clay under monotonic and cyclic loading. *Geotextiles and Geomembranes*, **20**, No. 2, 117–133.

Valentine, R. J. (2013). An assessment of the factors that contribute to the poor performance of geosynthetic-reinforced earth retaining walls. *Design and Practice of Geosynthetic-Reinforced Soil Structures*, Ling, H.I., Guido, G., Daniele, C., Jie, H. & Tatsuoka, F., Editors, DESTech Publications, Bologna, Italy, pp. 318–327.

van Genuchten, M. Th. (1980). A closed-form equation for predicting the hydraulic conductivity of unsaturated soils. *Soil Science Society of America Journal*, **44**, No. 5, 892–898.

Yoo, C. & Jung, H. Y. (2006). Case history of geosynthetic reinforced segmental retaining wall failure. *Journal of Geotechnical and Geoenvironmental Engineering*, **132**, No. 12, 1538–1548.

Zornberg, J. G. & Mitchell, J. K. (1994). Reinforced soil structures with poorly draining backfills. Part I: reinforcement interactions and functions. *Geosynthetics International*, **1**, No. 2, 103–148.

Zornberg, J. G., Bouazza, A. & McCartney, J. S. (2010). Geosynthetic capillary barriers: current state of knowledge. *Geosynthetics International*, **17**, No. 5, 273–300.

The Editor welcomes discussion on all papers published in Geosynthetics International. Please email your contribution to discussion@geosynthetics-international.com 15 June 2016.